Electronic version of an article published as **International Journal of Structural Stability and Dynamics** (2020), 2043008 DOI: 10.1142/S0219455420430087 © 2020 World Scientific Publishing Company, https://www.worldscientific.com/doi/abs/10.1142/S0219455420430087

Postprint of: Kreja I., Sabik A., Equivalent Single Layer Models in Free Vibration Analysis of Laminated Multi-Layered Plates, International Journal of Structural Stability and Dynamics (2020), 2043008

Ireneusz KREJA[1], Agnieszka SABIK

EQUIVALENT SINGLE LAYER MODELS IN FREE VIBRATION ANALYSIS OF LAMINATED MULTI-LAYERED PLATES

Gdansk University of Technology, Faculty of Civil and Environmental Engineering,
G. Narutowicza 11/12, 80-233 Gdańsk, Poland,
e-mail: ireneusz.kreja@pg.edu.pl, agnieszka.sabik@pg.edu.pl

Abstract- The performance of selected Equivalent Single-Layer (ESL) models is evaluated within several classical benchmark tests for small amplitude free vibration analysis of multi-layered plates. The authors elaborated their own Finite Element software based on the first-order shear deformation theory (FOSD) with some modifications incorporated including a correction of the transverse shear stiffness and an application of zig-zag type functions. Seven different ESL models were considered in the study; beside the classical FOSD model, there were three FOSD models with various transverse shear corrections and three ESL models enhanced by the application of zig-zag functions and based on the Reissner's Mixed Variational Theorem.

Keywords: multi-layered plates; computational models; shear correction; zig-zag functions; free vibration

Dedication - This work is dedicated to Professor Junuthula N. Reddy on the occasion of his 75th anniversary. Professor Reddy's publications have been a remarkable inspiration for many researchers, including the authors of this work, to explore the secrets of composite panels' analysis.

1. Introduction

Since the publication of the meaningful paper of Mindlin [1] it is commonly acknowledged that the effect of the transverse shear deformation and rotatory inertia should be included in the flexural vibration analysis of moderately thick plates. Although theories of moderately thick plates could also be found in papers published before [1] e.g. by Reissner [2, 3] and Hencky [4], but it was Mindlin who was the first to consider the effects of rotational inertia and shear in the analysis of plates (cf. [5]). The plate theory accounting for those effects

[1] Corresponding Author, e-mail: ireneusz.kreja@pg.edu.pl, Tel.: +48 583471180

usually identified as the First Order Shear Deformation (FOSD) theory (or even more frequently, though not quite properly as the Mindlin-Reissner plate theory - cf. [6]) became a standard formulation for the bending analysis of moderately thick isotropic plates. However, already 100 years ago Timoshenko [7] indicated that the FOSD theory suffers from an overestimation of the transverse shear energy what implies a need to apply special correction for the transverse shear stiffness. The shear correction factor $\kappa = 5/6$ is commonly employed in FOSD models used in the static bending analysis of isotropic plates. This particular value can be deducted from the Reissner proposal [2], but also can be attained by matching the transverse shear strain energy predicted by the FOSD model with that obtained from the three-dimensional elasticity theory. An alternative approach was adopted by Mindlin [1], who suggested a slightly smaller number $\kappa = \pi^2/12$ based on the consideration of shear wave velocities calculated using the FOSD model and the three-dimensional approach. Yang et al. [8] initiated the use of FOSD models also in the analysis of heterogeneous anisotropic plates with particular emphasis on multi-layered panels. The shear effect is important in the analysis of fiber-reinforced polymer composite (FRPC) laminates, regardless of their thickness, which is due to the fact that while the material properties of FRPC in the direction of the fibers are determined by the characteristics of the reinforcement, their material properties in the thickness direction are dominated by a much weaker and more flexible polymer matrix [9, 10]. Consideration of rotational inertia seems particularly important in the analysis of sandwich structures. These two factors have determined the widespread use of FOSD models in the analysis of composite and sandwich panels [11]; however, it was required to apply the appropriate shear correction depending on the layering structure [12, 13]. In 1984, Reddy [14] presented his Third Order Shear Deformation (TOSD) theory without need to use any shear correction coefficients, but with parabolic distribution of transverse shear strains across the plate thickness and the transverse shear stresses vanishing on the top and bottom surfaces. However, no increase in the degree of interpolation of the displacement field over the thickness of the plate is able to map

the characteristic zig-zag deformation profile of a multi-layered plate with visible changes in the slope on the layer interfaces. This phenomenon resulted from the discontinuity of material properties in layered structures and the significant shear compliance of FRPC could be observed experimentally in many laminates. Such deformation pattern should be accompanied by a corresponding piecewise profile of stresses. A pertinent zig-zag deformation profile can be incorporated into the kinematic model of the layered plate by introducing some additional warping functions with a different slope in each layer [15]. However, a similar zig-zag effect can be noticed also in some stress based formulations (see e.g. Ambartsumyan [16]). A relevant zig-zag theory for multi-layered plates was proposed in 1986 by Murakami [17]. A noteworthy synthesis encompassing all the above-mentioned theories for multi-layered plates, which can be classified as equivalent single-layer (ESL) models, was presented by Reddy [18]. In more advanced computational models named discrete-layer (DL) theories or the layer-wise (LW) formulations a multi-layered plate is considered as a stack of laminas bounded together by appropriate conditions at ply interfaces [10]. The results obtained with the LW (DL) approach are very close to the results of 3D analysis [19]; however, due to the fact that the number of degrees of freedom in LW (DL) models directly depends on the number of layers, the final number of unknowns in the analysis of multi-layered plates using such models is many times higher than the number of unknowns within the ESL approach. This condition is a main reason that the use of LW (DL) models is in practice limited to the analysis of simple examples. Undoubtedly, it seems more attractive to combine both those approaches with the dominant involvement of ESL models, while LW (DL) modeling would be used only in selected regions of the plate [20].

In their earlier work [21], the authors examined performance of selected ESL models in a linear static Finite Element Analysis of multi-layered plates by confronting the obtained results with the available 3D analysis solutions. As one could expect, the computational models enhanced by the application of the zig-zag functions generally performed better than FOSD

models; however, FOSD models with a global (cross-sectional) transverse shear correction also did unexpectedly well. In the current work, a similar investigation has been carried out in the natural vibrations analysis of multi-layered panels.

2. Plate models considered in the current study

Within the general ESL formulation considered in the current report the entire multi-layered laminate is represented by a single-layer plate where the variation of the displacement through the plate thickness can be described as

$$\{\mathbf{U}(x,\ y,\ z)\} = [\mathbf{\Phi}(z)]\{\mathbf{u}(x,\ y)\}, \tag{1}$$

with the following notation:

$$\{\mathbf{U}(x,\ y,\ z)\} = \begin{Bmatrix} U(x,\ y,\ z) \\ V(x,\ y,\ z) \\ W(x,\ y,\ z) \end{Bmatrix} \qquad \text{and} \qquad \{\mathbf{u}(x,\ y)\} = \begin{Bmatrix} u(x,\ y) \\ v(x,\ y) \\ w(x,\ y) \\ \varphi_x(x,\ y) \\ \varphi_y(x,\ y) \\ \psi_x(x,\ y) \\ \psi_y(x,\ y) \end{Bmatrix}, \tag{2}$$

In the classical FOSD formulation [10] the displacement distribution through the plate thickness is taken as

$$\begin{aligned} U(x,\ y,\ z) &= u(x,\ y) + z\cdot\varphi_x(x,\ y) \\ V(x,\ y,\ z) &= v(x,\ y) + z\cdot\varphi_y(x,\ y)\ , \\ W(x,\ y,\ z) &= w(x,\ y) \end{aligned} \tag{3}$$

where u, v, and w are usual translational displacement components at the mid-surface, with φ_x and φ_y standing for rotational components.

The deformation profile (3) can be furtherly enhanced by adding appropriate zig-zag functions $\phi_\alpha{}^{(k)}(z)$, $\alpha = x, y$ (see Fig. 1) which represent the through-the-thickness warping effects:

$$\begin{aligned} U(x,\ y,\ z) &= u(x,\ y) + z\cdot\varphi_x(x,\ y) + \phi_x^{(k)}(z)\cdot\psi_x(x,\ y) \\ V(x,\ y,\ z) &= v(x,\ y) + z\cdot\varphi_y(x,\ y) + \phi_y^{(k)}(z)\cdot\psi_y(x,\ y), \\ W(x,\ y,\ z) &= w(x,\ y) \end{aligned} \tag{4}$$

with ψ_x and ψ_y being two supplementary unknown parameters that can be identified as the weighted-over-thickness amplitudes of the zig-zag effects.

For a general ESL formulation (1), which can cover the models given by equations (3, 4) one should assume

$$\left[\mathbf{\Phi}(z)\right]=\begin{bmatrix}1 & 0 & 0 & z & 0 & \phi_x^{(k)}(z) & 0\\ 0 & 1 & 0 & 0 & z & 0 & \phi_y^{(k)}(z)\\ 0 & 0 & 1 & 0 & 0 & 0 & 0\end{bmatrix}. \tag{5}$$

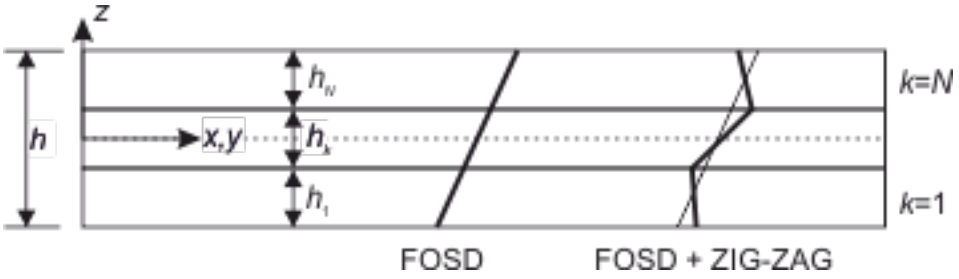

Fig. 1 First Order Shear Deformation model enhanced by Zig-zag function

According to the ESL concept the multi-layered medium is replaced by a single-layer plate with resultant stiffness obtained via the integration of the mechanical properties over the laminate thickness. The multi-layered plate is built of orthotropic layers with the following constitutive relations between stress and strain (assuming plane stress condition) [9, 10]

$$\begin{aligned}\left\{\boldsymbol{\sigma}_B(x,\,y,\,z)\right\}&=\begin{Bmatrix}\sigma_{xx}(x,\,y,\,z)\\ \sigma_{yy}(x,\,y,\,z)\\ \sigma_{xy}(x,\,y,\,z)\end{Bmatrix}=\begin{bmatrix}c_{11} & c_{12} & c_{13}\\ c_{12} & c_{22} & c_{23}\\ c_{13} & c_{23} & c_{33}\end{bmatrix}\begin{Bmatrix}\varepsilon_{xx}(x,\,y,\,z)\\ \varepsilon_{yy}(x,\,y,\,z)\\ \gamma_{xy}(x,\,y,\,z)\end{Bmatrix}=\left[\mathbf{C}_B\right]\left\{\boldsymbol{\varepsilon}_B(x,\,y,\,z)\right\},\\ \left\{\boldsymbol{\sigma}_S(x,\,y,\,z)\right\}&=\begin{Bmatrix}\sigma_{zx}(x,\,y,\,z)\\ \sigma_{yz}(x,\,y,\,z)\end{Bmatrix}=\begin{bmatrix}\tilde{c}_{55} & \tilde{c}_{45}\\ \tilde{c}_{45} & \tilde{c}_{44}\end{bmatrix}\begin{Bmatrix}\gamma_{zx}(x,\,y,\,z)\\ \gamma_{yz}(x,\,y,\,z)\end{Bmatrix}=\left[\tilde{\mathbf{C}}_S\right]\left\{\boldsymbol{\varepsilon}_S(x,\,y,\,z)\right\},\end{aligned} \tag{6}$$

where $\{\boldsymbol{\sigma}\}$ and $\{\boldsymbol{\varepsilon}\}$ represent vectors of stresses and strains; subscripts *B* and *S* refer to bending and shear components, respectively. Elements of the constitutive matrix marked with the tilde ($\tilde{\square}$) in (6) represent the transverse shear stiffness that requires a special correction in the FOSD

model. As mentioned earlier in Chapter 1 it can be modified by the *local* transverse shear correction factor κ:

$$\tilde{c}_{ij} = \kappa\, c_{ij} \tag{7}$$

This *local* transverse shear correction factor κ in (7) is introduced at the layer level. It is an alternative to the *global* (cross-sectional) transverse shear correction factors which can be derived from suitable assumptions valid for the entire multi-layered cross-section, described in the following.

The transverse shear forces can be obtained from the through-the-thickness integration of the appropriate stress components

$$\mathrm{T}_{xz} = \int_{-\frac{h}{2}}^{\frac{h}{2}} \sigma_{xz}\, dz, \quad \mathrm{T}_{yz} = \int_{-\frac{h}{2}}^{\frac{h}{2}} \sigma_{yz}\, dz. \tag{8}$$

These resultants can be expressed as a function of the transverse shear strains:

$$\begin{Bmatrix} \mathrm{T}_{xz} \\ \mathrm{T}_{yz} \end{Bmatrix} = \begin{bmatrix} \tilde{a}_{55} & \tilde{a}_{45} \\ \tilde{a}_{45} & \tilde{a}_{44} \end{bmatrix} \begin{Bmatrix} \gamma_{xz} \\ \gamma_{yz} \end{Bmatrix}, \tag{9}$$

where $\tilde{a}_{ij}$ $(i, j = 4, 5)$ stands for the transverse shear stiffness of the whole laminate. This stiffness can be estimated from the following relations:

$$\tilde{a}_{55} = (k_1)^2 \int_{-\frac{h}{2}}^{\frac{h}{2}} c_{55}\, dz, \quad \tilde{a}_{45} = k_1 k_2 \int_{-\frac{h}{2}}^{\frac{h}{2}} c_{45}\, dz, \qquad \tilde{a}_{44} = (k_2)^2 \int_{-\frac{h}{2}}^{\frac{h}{2}} c_{44}\, dz\,, \tag{10}$$

where k_1, and k_2 denote the *global* composite transverse shear correction factors. They are dependent on material properties as well as on stacking sequence of the layers and their orientation angles (see e.g. [12, 13]). The values of k_1, and k_2 follow from matching the transverse shear strain energy estimated by the FOSD plate model with that obtained from the 3D elasticity theory by making use of the assumption of a cylindrical bending mode of the plate and by utilizing the differential relation between the resulting transverse shear forces and bending moments. Rolfes & Rohwer [22] implemented an ”improved transverse shear

stiffness" in their modified FOSD model. They evaluated the effective transverse shear stiffness based on similar assumptions as those applied in [12, 13]; however, the final results are slightly different; mainly due to an independent evaluation of the stiffness term $\tilde{a}_{45}$. The results provided by both those approaches for static tests performed in [21] were almost identical for the most of the considered examples, therefore only the concept of Rolfes & Rohwer [22] has been examined in the current research.

The linear strain components within general ESL formulation can be obtained as appropriate derivatives of the displacements:

$$\begin{aligned}
\varepsilon_{xx}(x,\,y,\,z) &= \frac{\partial U(x,\,y,\,z)}{\partial x} \\
\varepsilon_{yy}(x,\,y,\,z) &= \frac{\partial V(x,\,y,\,z)}{\partial y} \\
\gamma_{xy}(x,\,y,\,z) &= \frac{\partial U(x,\,y,\,z)}{\partial y} + \frac{\partial V(x,\,y,\,z)}{\partial x} \\
\gamma_{xz}(x,\,y,\,z) &= \frac{\partial U(x,\,y,\,z)}{\partial z} + \frac{\partial W(x,\,y,\,z)}{\partial x} \\
\gamma_{yz}(x,\,y,\,z) &= \frac{\partial V(x,\,y,\,z)}{\partial z} + \frac{\partial W(x,\,y,\,z)}{\partial y}
\end{aligned} \tag{11}$$

The first three equations of (11) representing the in-plane strain components can be given as

$$\left\{\boldsymbol{\varepsilon}_B(x,\,y,\,z)\right\} = \left[\boldsymbol{\Lambda}(z)\right]\left[\mathbf{B}_{B0}\right]\left\{\mathbf{u}(x,\,y)\right\}. \tag{12}$$

with

$$\left[\boldsymbol{\Lambda}(z)\right] = \begin{bmatrix} 1 & 0 & 0 & z & 0 & 0 & \phi_x^{(k)}(z) & 0 & 0 & 0 \\ 0 & 1 & 0 & 0 & z & 0 & 0 & \phi_y^{(k)}(z) & 0 & 0 \\ 0 & 0 & 1 & 0 & 0 & z & 0 & 0 & \phi_x^{(k)}(z) & \phi_y^{(k)}(z) \end{bmatrix}, \tag{13}$$

$$\left[\mathbf{B}_{B0}\right]=\begin{bmatrix} \partial/\partial x & 0 & 0 & 0 & 0 & 0 & 0 \\ 0 & \partial/\partial y & 0 & 0 & 0 & 0 & 0 \\ \partial/\partial y & \partial/\partial x & 0 & 0 & 0 & 0 & 0 \\ 0 & 0 & 0 & \partial/\partial x & 0 & 0 & 0 \\ 0 & 0 & 0 & 0 & \partial/\partial y & 0 & 0 \\ 0 & 0 & 0 & \partial/\partial y & \partial/\partial x & 0 & 0 \\ 0 & 0 & 0 & 0 & 0 & \partial/\partial x & 0 \\ 0 & 0 & 0 & 0 & 0 & 0 & \partial/\partial y \\ 0 & 0 & 0 & 0 & 0 & \partial/\partial y & 0 \\ 0 & 0 & 0 & 0 & 0 & 0 & \partial/\partial x \end{bmatrix} \tag{14}$$

and

$$\left\{\mathbf{u}(x,\,y)\right\}^T=\left\{u \quad v \quad w \quad \varphi_x \quad \varphi_y \quad \psi_x \quad \psi_y\right\}. \tag{15}$$

Accordingly, the transverse shear strain components can be presented as:

$$\gamma_{\alpha z}(x,\,y,\,z)=\varphi_\alpha(x,\,y)+\frac{\partial w(x,\,y)}{\partial\alpha}+\frac{\partial\phi_\alpha^{(k)}(z)}{\partial z}\,\psi_\alpha(x,\,y),\quad \alpha=x,y. \tag{16}$$

From (16) it appears, that only the last component depends on the variable z and the choice of a particular warping function. Analogously to [21], the following two options of the warping function are considered in the current report:

1) the zig-zag function of Murakami [17]:

$$\begin{gathered} \phi_x^{(k)}(z)=\phi_y^{(k)}(z)=f(z)=(-1)^k\zeta_k, \\ z\in\left\langle z_{(k-1)},z_k\right\rangle,\quad z_0=-0.5h,\quad z_k=z_{(k-1)}+h_k, \\ k=1...,N \end{gathered} \tag{17}$$

where h_k is the thickness of the k^{th} layer and ζ_k is the local dimensionless coordinate of the k^{th} layer:

$$\zeta_k=2\frac{z-z_k}{h_k}+1,\quad \zeta_k\in\left\langle -1,1\right\rangle,\qquad k=1...,N\,. \tag{18}$$

2) the zig-zag function of Tessler et al. [23]:

$$\phi_\alpha^{(1)} = (z+0.5h)\left(\frac{G_\alpha}{Q_{\alpha\alpha}^{(1)}}-1\right) \qquad k=1$$
$$\phi_\alpha^{(k)} = (z+0.5h)\left(\frac{G_\alpha}{Q_{\alpha\alpha}^{(k)}}-1\right)+\sum_{i=2}^{k} h^{(i-1)}\left(\frac{G_\alpha}{Q_{\alpha\alpha}^{(i-1)}}-\frac{G_\alpha}{Q_{\alpha\alpha}^{(k)}}\right) \qquad k=2,....,N \tag{19}$$
$$z\in\left\langle z_{(k-1)}, z_k\right\rangle, \quad z_0=-0.5h, \quad z_k=z_{(k-1)}+h_k, \quad k=1...,N, \quad \alpha=x,y$$

where N indicates the total number of layers and $k \in \langle 1, N\rangle$ identifies the number of the current layer; $Q^{(k)}_{\alpha\alpha}$ stands for the diagonal coefficients of the constitutive matrix for the k^{th} layer ($Q_{xx} = c_{55}$ and $Q_{yy} = c_{44}$). The weighted-average transverse shear stiffness coefficients G_α follow from

$$G_\alpha = \left(\frac{1}{h}\int_{-0.5h}^{0.5h}\frac{dz}{Q_{\alpha\alpha}^{(k)}}\right)^{-1} = \left(\frac{1}{h}\sum_{k=1}^{N}\frac{h_k}{Q_{\alpha\alpha}^{(k)}}\right)^{-1}, \quad \alpha=x,y. \tag{20}$$

One can notice, that the derivatives of the above mentioned zig-zag functions with respect to the coordinate z are constant over the thickness of the layer:

a) for the zig-zag function of Murakami (17):

$$\frac{\partial\phi_x^{(k)}(z)}{\partial z} = \frac{\partial\phi_y^{(k)}(z)}{\partial z} = (-1)^k\cdot\frac{2}{h_k}. \tag{21}$$

b) for the zig-zag function of Tessler et al. (19):

$$\begin{aligned}\frac{\partial\phi_x^{(k)}(z)}{\partial z} &= \frac{G_x}{Q_{xx}^{(k)}}-1\\ \frac{\partial\phi_y^{(k)}(z)}{\partial z} &= \frac{G_y}{Q_{yy}^{(k)}}-1\end{aligned}. \tag{22}$$

Consequently, the transverse shear strains remain constant over the thickness of the layer:

$$\left\{\boldsymbol{\varepsilon}_S(x,\,y,z)\right\} \Leftrightarrow \left\{\boldsymbol{\varepsilon}_S^{(k)}(x,\,y)\right\} = \left[\mathbf{B}_S^{(k)}(x,\,y)\right]\left\{\mathbf{u}(x,\,y)\right\} \tag{23}$$

with

$$\left[\mathbf{B}_S^{(k)}(x,\ y)\right]=\begin{bmatrix} 0\ 0\ \partial/\partial x\ 1\ 0\ \dfrac{\partial \phi_x^{(k)}}{\partial z} & 0 \\ 0\ 0\ \partial/\partial y\ 0\ 1\ \ 0 & \dfrac{\partial \phi_y^{(k)}}{\partial z} \end{bmatrix}. \tag{24}$$

The motion equations of the FE displacement formulation can be derived from D'Alembert's form of the *Principle of Virtual Displacement* (PVD) where the virtual work of external forces

$$\delta W_{ext}=\{\delta\mathbf{q}\}^T\{\mathbf{P}\}+\int_A\{\delta\mathbf{u}(x,y)\}^T\{\mathbf{t}(x,y)\}dA+\int_V\{\delta\mathbf{U}(x,y,z)\}^T\{\mathbf{f}_B(x,y,z)\}dV \tag{25}$$

include inertia forces

$$\{\mathbf{f}_B(x,y,z)\}=-\rho\{\ddot{\mathbf{U}}(x,y,z)\}=-\rho[\mathbf{\Phi}(z)]\{\ddot{\mathbf{u}}(x,\ y)\} \tag{26}$$

with $\{\delta\mathbf{u}\}$ and $\{\delta\mathbf{q}\}$ standing for, respectively, variations of the mid-plane displacements and variations of nodal displacements; while $\{\mathbf{P}\}$ represents nodal forces, $\{\mathbf{t}\}$ is a vector of surface tractions and ρ is a mass density that can be different in various laminate layers.

The internal virtual work, δW_{in}, for the layered plate is

$$\delta W_{in}=\int_A\left(\sum_{k=1}^{N}\left(\int_{z_{(k-1)}}^{z_k}\left(\{\delta\boldsymbol{\varepsilon}_B\}^T\{\boldsymbol{\sigma}_B\}+\{\delta\boldsymbol{\varepsilon}_S\}^T\{\boldsymbol{\sigma}_{S(a)}\}\right)dz\right)\right)dA, \tag{27}$$

where $\{\boldsymbol{\sigma}\}$ and $\{\delta\boldsymbol{\varepsilon}\}$ represent vectors of stresses and virtual strains; subscripts *B* and *S* refer to bending and shear components, respectively.

With an appropriate interpolation of displacement unknowns

$$\{\mathbf{u}(x,\ y)\}=[\mathbf{N}(x,\ y)]\{\mathbf{q}\}, \tag{28}$$

where $[\mathbf{N}(x, y)]$ stands for shape functions matrix and $\{\mathbf{q}\}$ is the vector of nodal displacements, the virtual strain and stress fields can be expressed with the standard formulas:

$$\{\delta\boldsymbol{\varepsilon}_B\}^T=\{\delta\mathbf{q}\}^T[\mathbf{N}(x,\ y)]^T[\mathbf{B}_{B0}]^T[\mathbf{\Lambda}(z)]^T, \tag{29}$$

$$\{\delta\boldsymbol{\varepsilon}_S\}^T=\{\delta\mathbf{q}\}^T[\mathbf{N}(x,\ y)]^T[\mathbf{B}_S^{(k)}(x,\ y)]^T, \tag{30}$$

$$\{\boldsymbol{\sigma}_B\} = [\mathbf{C}_B][\boldsymbol{\Lambda}(z)][\mathbf{B}_{B0}][\mathbf{N}(x,\, y)]\{\mathbf{q}\}, \tag{31}$$

$$\{\boldsymbol{\sigma}_S\} = [\mathbf{C}_S]\left[\mathbf{B}_S^{(k)}(x,\, y)\right][\mathbf{N}(x,\, y)]\{\mathbf{q}\}. \tag{32}$$

With expressions (29-32) the formula for the internal virtual work of the layered plate (27) can be transformed to

$$\delta W_{in} = \{\delta\mathbf{q}\}^T [\mathbf{K}]\{\mathbf{q}\}, \tag{33}$$

where $\{\mathbf{q}\}$ is the global vector of displacements and $[\mathbf{K}]$ stands for the global stiffness matrix:

$$\begin{aligned}[\mathbf{K}] = \sum_{el=1}^{N_{el}} \Bigg(\int_{A_{el}} \Bigg([\mathbf{N}]^T [\mathbf{B}_{B0}]^T \sum_{k=1}^{N} \Bigg(\int_{z_{(k-1)}}^{z_k} [\boldsymbol{\Lambda}(z)]^T [\mathbf{C}_B][\boldsymbol{\Lambda}(z)]\, dz \Bigg) [\mathbf{B}_{B0}][\mathbf{N})] \Bigg) dA_{el} \\ + \int_{A_{el}} \Bigg([\mathbf{N}]^T \sum_{k=1}^{N} \Bigg(\left[\mathbf{B}_S^{(k)}\right]^T \int_{z_{(k-1)}}^{z_k} [\mathbf{C}_S]\, dz \left[\mathbf{B}_S^{(k)}\right] \Bigg) [\mathbf{N})] \Bigg) dA_{el} \Bigg).\end{aligned} \tag{34}$$

From (27) one can deduce the following interpolation of accelerations

$$\{\ddot{\mathbf{u}}(x,\, y)\} = [\mathbf{N}(x,\, y)]\{\ddot{\mathbf{q}}\}, \tag{35}$$

and then the virtual work of external forces can be presented as

$$\delta W_{ext} = \{\delta\mathbf{q}\}^T \left(\{\mathbf{P}\} + \sum_{el=1}^{N_{el}} \left(\int_{A_{el}} [\mathbf{N}]^T \{\mathbf{t}\}\, dA_{el} \right) - [\mathbf{M}]\{\ddot{\mathbf{q}}\} \right). \tag{36}$$

In (36) the first two components are related to the concentrated forces and surface loads, and the last component represents the inertia forces, with the global mass matrix given as:

$$[\mathbf{M}] = \sum_{el=1}^{N_{el}} \left(\int_{A_{el}} [\mathbf{N}(x,\, y)]^T \left(\sum_{k=1}^{N} \left(\int_{z_{(k-1)}}^{z_k} \rho [\mathbf{\Phi}(z)]^T [\mathbf{\Phi}(z)] dz \right) \right) [\mathbf{N}(x,\, y)] dA_{el} \right)$$

$$= \sum_{el=1}^{N_{el}} \left(\int_{A_{el}} [\mathbf{N}]^T \begin{bmatrix} I_0 & 0 & 0 & I_1 & 0 & J_{x0}^1 & 0 \\ 0 & I_0 & 0 & 0 & I_1 & 0 & J_{y0}^1 \\ 0 & 0 & I_0 & 0 & 0 & 0 & 0 \\ I_1 & 0 & 0 & I_2 & 0 & J_{x1}^1 & 0 \\ 0 & I_1 & 0 & 0 & I_2 & 0 & J_{y1}^1 \\ J_{x0}^1 & 0 & 0 & J_{x1}^1 & 0 & J_{x0}^2 & 0 \\ 0 & J_{y0}^1 & 0 & 0 & J_{y1}^1 & 0 & J_{y0}^2 \end{bmatrix} [\mathbf{N}] dA_{el} \right). \quad (37)$$

Formulas for the inertia components given in (37) can be found in the Appendix A.

Finally, with (33) and (36) one can arrive at the classical form of the motion equation governing undamped forced vibrations of linear systems:

$$[\mathbf{K}]\{\mathbf{q}\} + [\mathbf{M}]\{\ddot{\mathbf{q}}\} = \{\mathbf{R}\}, \quad (38)$$

where vector {**R**} represents all excitation forces. Assuming zero excitations and harmonic form of dynamical deflections one can easy transform (38) to the standard eigenvalue problem equation describing natural free vibrations:

$$\left([\mathbf{K}] - \omega^2 [\mathbf{M}] \right) \{\mathbf{A}\} = \{\mathbf{0}\}, \quad (39)$$

where ω indicates the circular frequency of free vibrations and {**A**} represents the eigenvector describing the corresponding vibration mode.

Before proceeding to practical applications of equation (39), let's consider alternative FE formulation to the displacement version given by (27). By assuming a mixed variational formulation with an independent interpolation of transverse stress components as proposed by Reissner [24] and known in the literature as *Reissner's Mixed Variational Theorem* (RMVT), one can ensure the interlayer shear stress continuity and zero transverse shear stresses on the top and bottom surfaces. Murakami [17] constructed his theory for laminated plates by assuming the FOSD hypothesis for each individual layer of the multi-layered plate, but, due to

implementation of the RMVT he could impose the parabolic distribution of the transverse shear stress components in each layer and simultaneously ensure the inter-laminar stresses continuity. This approach was also followed by others, see *e.g.* [25, 26].

The variation of the internal work in the plate built of N layers within the framework of RMVT can be expressed as:

$$\delta W_{in} = \int_A \left(\sum_{k=1}^{N} \left(\int_{z_{(k-1)}}^{z_k} \left(\{\delta\boldsymbol{\varepsilon}_B\}^T \{\boldsymbol{\sigma}_B\} + \{\delta\boldsymbol{\varepsilon}_S\}^T \{\boldsymbol{\sigma}_{S(a)}\} + \{\delta\boldsymbol{\sigma}_{S(a)}\}^T \left(\{\boldsymbol{\varepsilon}_S - \boldsymbol{\varepsilon}_{S(a)}\} \right) \right) dz \right) \right) dA, \quad (40)$$

with k standing for the layer number, h_k being the thickness of the k^{th} layer, $\boldsymbol{\varepsilon}$ and $\boldsymbol{\sigma}$ representing strains and stresses, where subscripts B and S refer to bending and shear components, correspondingly. An additional subscript *(a)* is used for the assumed field of transverse shear stresses and the related field of transverse shear strains (via Hooke's law).

The first and the second components in (40) denote the internal energy associated with bending and the transverse shear of the plate, respectively. In variational sense they match the equilibrium condition. The third term on the other hand expresses variationally the compatibility of the transverse shear stresses.

The transverse shear stress $\boldsymbol{\sigma}_{S(a)}$ in (40) can adopt various distribution in the plate thickness direction. In the current research, a quadratic distribution of transverse shear stresses is assumed in each layer after [17] as

$$\sigma_{\alpha z}^{(k)}(z) = F_{top}\, \sigma_{\alpha z}^{top(k)} + F_m\, \mathrm{T}_{\alpha z}^{(k)} + F_{bot}\, \sigma_{\alpha z}^{bot(k)}, \quad \alpha = x, y, \quad (41)$$

with $\sigma_{\alpha z}^{top(k)}$ and $\sigma_{\alpha z}^{bot(k)}$ signifying the transverse shear stress at the top and bottom surfaces of the layer k, and $\mathrm{T}_{\alpha z}^{(k)}$ indicating the corresponding resultant forces for the layer k

$$\mathrm{T}_{\alpha z}^{(k)} = \int_{z_{(k-1)}}^{z_k} \sigma_{\alpha z}\, dz, \quad \alpha = x, y. \quad (42)$$

F_{top}, F_{m} and F_{bot} are the stress interpolation functions which have a form:

$$F_{top}\left(\xi_k\right)=-\frac{1}{4}+\frac{\xi_k}{2}+\frac{3}{4}\xi_k{}^2;\quad F_m\left(\xi_k\right)=\frac{3\cdot\left(1-\xi_k{}^2\right)}{2\cdot h_k};\quad F_{bot}\left(\xi_k\right)=-\frac{1}{4}-\frac{\xi_k}{2}+\frac{3}{4}\xi_k{}^2. \quad (43)$$

The stress variables can be eliminated from the set of unknowns by invoking the stress continuity requirements at layer interfaces:

$$\sigma_{xz}^{top(k)}=\sigma_{xz}^{bot(k+1)}\qquad \sigma_{yz}^{top(k)}=\sigma_{yz}^{bot(k+1)}\qquad k=1,2,...N-1, \quad (44)$$

and zeroing of transverse shear stress at the top and the bottom surfaces:

$$\sigma_{xz}(z=\pm h/2)=0\qquad \sigma_{yz}(z=\pm h/2)=0\,. \quad (45)$$

As a consequence, one can obtain a pure displacement based model with seven kinematical unknown parameters as presented in (4) (*cf.* [17, 21, 25, 26]).

The set of computational models examined in the current study consists of seven formulations presented in Table 1.

Table 1. Considered computational models

Tag	Transverse shear deformation	Variational formulation	Number of unknowns at single node	Transverse shear stress continuity
FOSD_0	"pure" FOSD model without transverse shear correction	PVD (27)	5	NO
FOSD_1M	FOSD with the *local* shear correction factor $\kappa = \pi^2/12$ for every layer in (7) after Mindlin [1]	PVD (27)	5	NO
FOSD_1R	FOSD with the *local* shear correction factor $\kappa = 5/6$ for every layer in (7) after Reissner [2]	PVD (27)	5	NO
FOSD_3	FOSD with *global* correction of composite transverse shear stiffness following Rolfes & Rohwer [22] (see Appendix B)	PVD (27)	5	NO
ZZ_1	zig-zag function (17) after Murakami [17]	RMVT (40)	7	YES
ZZ_2	zig-zag function (19) after Tessler [23]	PVD (27)	7	YES
ZZ_3	zig-zag function (19) after Tessler [23]	RMVT (40)	7	YES

3. Numerical Examples

Since, in the early 1970s, Srinivas et al. [27, 28] and Noor [29] presented their exact solutions to the problems of free vibrations of multi-layer plates obtained on the basis of the

three-dimensional theory of elasticity, their examples have been widely adopted as mandatory benchmarks for testing new computational models. Additional reference results could be found in Reddy & Kuppusamy [30] and Noor & Burton [31, 32], and more recently in Kulkarni & Kapuria [33]. Test examples taken from the aforementioned classic works have been used in this report to examine the performance of the selected ESL models in a small amplitude free vibration analysis of multi-layered plates. All own results presented in the current report have been calculated with the authors' own finite element software [26, 34] suitably supplemented by the implementation of the Bathe subspace iteration method for solving eigenvalue problem [35]. In the FE discretization, appropriately dense meshes of isoparametric Lagrangian 16-node finite elements were used to minimize the error of FEM approximation. Supplementary verification calculations were also performed using 9-node elements. Moreover, at the initial stage of preparing the FEA software, the correctness of solving the eigenvalue problem by the subspace iteration method was additionally positively verified using the SECANT procedure [35]; the results obtained with both methods were identical, but the computation times for the SECANT procedure were twice as long.

3.1. Simply supported three-layer orthotropic square plate

The first example to be considered in the present study is the classical benchmark problem introduced by Srinivas & Rao [28], who analyzed the change in the vibration fundamental frequency of a square ($a = b$) 3-layered simply supported orthotropic plate as a result of changing the stiffness of thinner covers ($h_1 = h_3 = 0.1\,h$, $h = 0.1\,a$) in relation to the constant modules of the thicker core ($h_2 = 0.8\,h$), with h standing for the total thickness. The following constitutive parameters (cf. (6)) can be determined for aragonite crystal ($CaC0_3$) used as a material of the inner layer [28]: $c_{11} = 0.999781\ \chi$; $c_{12} = 0.231141\ \chi$; $c_{22} = 0.524771\ \chi$; $c_{13} = c_{23} = 0.0$; $c_{33} = 0.262931\ \chi$; $c_{44} = 0.266810\ \chi$; $c_{55} = 0.159914\ \chi$; with $\chi = 160$ GPa. By multiplying these numbers by the factor β one can get the corresponding c_{ij} components for the material assigned to both the external layers.

The assumed boundary conditions (SSSS) fully match the set "SS-1" of simply support constraints defined by Reddy [10]:

$$\begin{aligned} u(x,\ 0) &= u(x,\ b) = 0 \\ v(0,\ y) &= v(a,\ y) = 0 \\ w(x,\ 0) &= w(0,\ y) = w(x,\ b) = w(a,\ y) = 0 \\ \varphi_x(x,\ 0) &= \varphi_x(x,\ b) = 0 \\ \varphi_y(0,\ y) &= \varphi_y(a,\ y) = 0 \\ \psi_x(x,\ 0) &= \psi_x(x,\ b) = 0 \\ \psi_y(0,\ y) &= \psi_y(a,\ y) = 0 \end{aligned} \quad , \tag{46}$$

The dimensionless frequency obtained for varying value of the modular ratio, β, and normalized according to [28] as

$$\lambda = \omega \sqrt{\frac{\rho h^2}{\chi}} \tag{47}$$

is presented in Table 2 and compared with the exact 3D solution provided by Srinivas & Rao [28].

Table 2. Natural vibration fundamental frequency for three-layer simply supported (SSSS) orthotropic plate

β	**FOSD_0**		**FOSD_1M**		**FOSD_1R**		**FOSD_3**	
	λ	*Error [%]*	λ	*Error [%]*	λ	*Error [%]*	λ	*Error [%]*
1	0.047698	*0.59*	0.047380	*-0.08*	0.047403	*-0.03*	0.047403	*-0.03*
2	0.057751	*1.25*	0.057283	*0.42*	0.057317	*0.48*	0.057017	*-0.04*
5	0.080362	*4.17*	0.079524	*3.08*	0.079585	*3.16*	0.077116	*-0.04*
10	0.107696	*9.78*	0.106405	*8.46*	0.106498	*8.56*	0.098049	*-0.06*
15	0.129279	*15.39*	0.127636	*13.93*	0.127754	*14.03*	0.111947	*-0.08*
β	**ZZ_1**		**ZZ_2**		**ZZ_3**		**Exact 3D** [28]	
	λ	*Error [%]*	λ	*Error [%]*	λ	*Error [%]*		
1	0.047403	*-0.03*	0.047403	*-0.03*	0.047403	*-0.03*	**0.047419**	
2	0.057078	*0.06*	0.057106	*0.11*	0.057078	*0.06*	**0.057041**	
5	0.077167	*0.02*	0.077193	*0.06*	0.077167	*0.02*	**0.077148**	
10	0.098109	*0.01*	0.098136	*0.03*	0.098109	*0.01*	**0.098104**	
15	0.112030	*0.00*	0.112056	*0.02*	0.112030	*0.00*	**0.112034**	

Srinivas & Rao [28] indicated that the error of the thin plate (CLT) approximation for the current example significantly increased with the increase of the modular ratio, β (from

4.74% for $\beta = 1$, to 24.06% for $\beta = 15$), therefore one should not be surprised to observe a similar tendency for the FOSD models. Although, by taking into account the transverse shear and rotational inertia, the **FOSD_0** model offers for a homogenous plate ($\beta = 1$) a notably better performance than CLT, but the error exceeds 15% for $\beta = 15$. This performance could not be significantly improved by the application of local shear correction factors κ (either models **FOSD_1M** or **FOSD_1R**). However, the global correction of composite transverse shear stiffness as applied in model **FOSD_3** worked much better and turned out to be almost as effective as application of zig-zag functions. When it comes to the zig-zag theories, it may be interesting to note that the values of 4 out of 8 inertia components $(J^1_{x1}, J^1_{y1}, J^2_{x0}, J^2_{y0})$ are distinctly different in the **ZZ_1** and **ZZ_3** models; however, the final solutions obtained with them, both in terms of frequency and vibration modes, were identical. In this example, one can observe a slight advantage of the RMVT-based models **ZZ_01** and **ZZ_03** over the PVD-based **ZZ_02**. It should also be noted that the frequency obtained for $\beta = 1$ with models **FOSD_3**, **ZZ_01**, **ZZ_02** and **ZZ_03** is identical to that obtained for **FOSD_1R**, which results from the features of these models when applied to single-layer boards.

3.2. Simply supported composite square plate

Kulkarni & Kapuria [33] provided exact 3D elasticity results for free vibrations of several rectangular multi-layered plates. The one considered in this example is a square simply-supported plate constructed as a symmetric cross-ply (0/90/90/0) composite laminate with 4 layers of equal thicknesses. The graphite-epoxy layer is characterized by the following material parameters: E_L = 181 GPa; E_T = 10.3 GPa; G_{LT} = 7.17 GPa; G_{TT} = 2.87 GPa; ν_{LT} = 0.28.

The first ten natural frequencies calculated for three different values of the length to thickness ratio (a/h) are tabularized in Table 3 with the application of the following normalization:

$$\lambda = \omega \frac{a^2}{h} \sqrt{\frac{\rho}{E_T}}. \tag{48}$$

One can observe that the exact 3D reference results [33] were provided only for the first five flexural vibration frequencies, while the set of boundary conditions (46) applied in computations allows also for in-plane vibration modes (frequencies enclosed in parentheses).

Table 3. Natural frequencies of simply supported (SSSS) square cross-ply (0/90/90/0) plate

a/h	mode	**FSDT_0**		**FSDT_1M**		**FSDT_1R**		**FSDT_3**		**ZZ_1 = ZZ_3**		**ZZ_2**		**Exact 3D** [33]
		λ	*Error [%]*	λ	*Error [%]*	λ	*Error [%]*	λ	*Error [%]*	λ	*Error [%]*	λ	*Error [%]*	
5	1	9.5256	*11.27*	9.1080	*6.39*	9.1366	*6.72*	8.4713	*-1.05*	8.5485	*-0.15*	8.6255	*0.75*	**8.5611**
	2	(13.1057)		(13.1057)		(13.1057)		(13.1057)		(13.1057)		(13.1057)		-
	3	(13.1057)		(13.1057)		(13.1057)		(13.1057)		(13.1057)		(13.1057)		-
	4	17.1251	*7.84*	16.3092	*2.70*	16.3654	*3.06*	15.6578	*-1.40*	15.8338	*-0.29*	16.1477	*1.69*	**15.8799**
	5	20.5641	*17.45*	19.0718	*8.93*	19.1701	*9.49*	16.8095	*-3.99*	17.4941	*-0.08*	17.7012	*1.10*	**17.5087**
	6	25.1694	*13.21*	23.5120	*5.76*	23.6223	*6.25*	21.4693	*-3.43*	22.1867	*-0.20*	22.5499	*1.43*	**22.2319**
	7	(26.2114)		26.0759	*1.79*	26.1898	*2.24*	25.1497	*-1.82*	25.5275	*-0.35*	26.2492	*2.47*	**25.6164**
	8	(26.2114)		(26.2114)		(26.2114)		25.3798		27.4067		27.8234		-
	9	27.7608	*8.37**	(26.2114)		(26.2114)		(26.2114)		30.0049		30.7226		-
	10	31.9006		29.2788		29.4494		(26.2114)		30.7569		31.2744		-
10	1	11.9284	*5.58*	11.6958	*3.52*	11.7123	*3.67*	11.2750	*-0.20*	11.2915	*-0.06*	11.3367	*0.34*	**11.2981**
	2	22.0567	*3.78*	21.5886	*1.58*	21.6219	*1.74*	21.1367	*-0.55*	21.2193	*-0.16*	21.4031	*0.71*	**21.2529**
	3	(26.2114)		(26.2114)		(26.2114)		(26.2114)		(26.2114)		(26.2114)		-
	4	(26.2114)		(26.2114)		(26.2114)		(26.2114)		(26.2114)		(26.2114)		-
	5	32.3621	*14.21*	30.7743	*8.60*	30.8828	*8.99*	28.0579	*-0.98*	28.3288	*-0.03*	28.5548	*0.77*	**28.3362**
	6	38.1024	*11.27*	36.4320	*6.39*	36.5465	*6.72*	33.8851	*-1.05*	34.1939	*-0.15*	34.5022	*0.75*	**34.2444**
	7	39.2862	*4.55*	38.0346	*1.22*	38.1227	*1.46*	37.2828	*-0.78*	37.4954	*-0.21*	38.0936	*1.38*	**37.5751**
	8	50.7240		48.5592		48.7085		46.1184		46.6019		47.2479		-
	9	(52.4229)		52.0650		52.3119		46.1386		47.2691		47.7537		-
	10	(52.4229)		(52.4229)		(52.4229)		50.2086		51.3447		51.8807		-
20	1	12.9501	*1.80*	12.8714	*1.18*	12.8771	*1.23*	12.7167	*-0.03*	12.7188	*-0.02*	12.7354	*0.11*	**12.7210**
	2	24.2798	*1.25*	24.1160	*0.57*	24.1279	*0.62*	23.9399	*-0.17*	23.9672	*-0.05*	24.0322	*0.22*	**23.9803**
	3	41.2158	*6.52*	40.3400	*4.25*	40.4024	*4.41*	38.6374	*-0.15*	38.6918	*-0.01*	38.8418	*0.38*	**38.6947**
	4	45.8192	*1.61*	45.2970	*0.45*	45.3347	*0.53*	44.9630	*-0.29*	45.0592	*-0.08*	45.3204	*0.50*	**45.0944**
	5	47.7139	*5.58*	46.7832	*3.52*	46.8495	*3.67*	45.1001	*-0.20*	45.1660	*-0.06*	45.3470	*0.34*	**45.1926**
	6	52.4229		(52.4229)		(52.4229)		(52.4229)		(52.4229)		(52.4229)		-
	7	52.4229		(52.4229)		(52.4229)		(52.4229)		(52.4229)		(52.4229)		-
	8	63.3390		62.1606		62.2447		60.5132		60.6701		61.0078		-
	9	74.9216		73.5986		73.6934		72.4677		72.8190		73.2775		-
	10	80.9489		77.9447		78.1540		72.8963		73.1098		73.8024		-

* Due to the transfer in vibration modes, this error value was calculated with respect to the 5th flexural frequency from the reference solution

By examining the error measures given in Table 3 one can judge that the basic FOSD model (**FOSD_0**), can provide an acceptable estimation only for the fundamental frequency of

the thinnest of considered plates ($a = 20\,h$). An improvement of results obtained by an application of the local transverse shear correction in models **FOSD_1M** and **FOSD_1R** is very limited. However, the global shear correction implemented in **FOSD_3** has been much more effective, what resulted in a very good performance of that model. Here again, both the zig-zag models based on the RMVT (**ZZ_1** and **ZZ_3**) gave identical numbers and an excellent agreement with the reference solution of Kulkarni & Kapuria [33]. The performance of model **ZZ_2** is slightly worse but the accuracy of the results calculated with this approach can be compared with that offered by **FOSD_3.**

Selected flexural vibration modes achieved with the zig-zag model **ZZ_1** for $a = 10\,h$ plate are presented in Fig. 2.

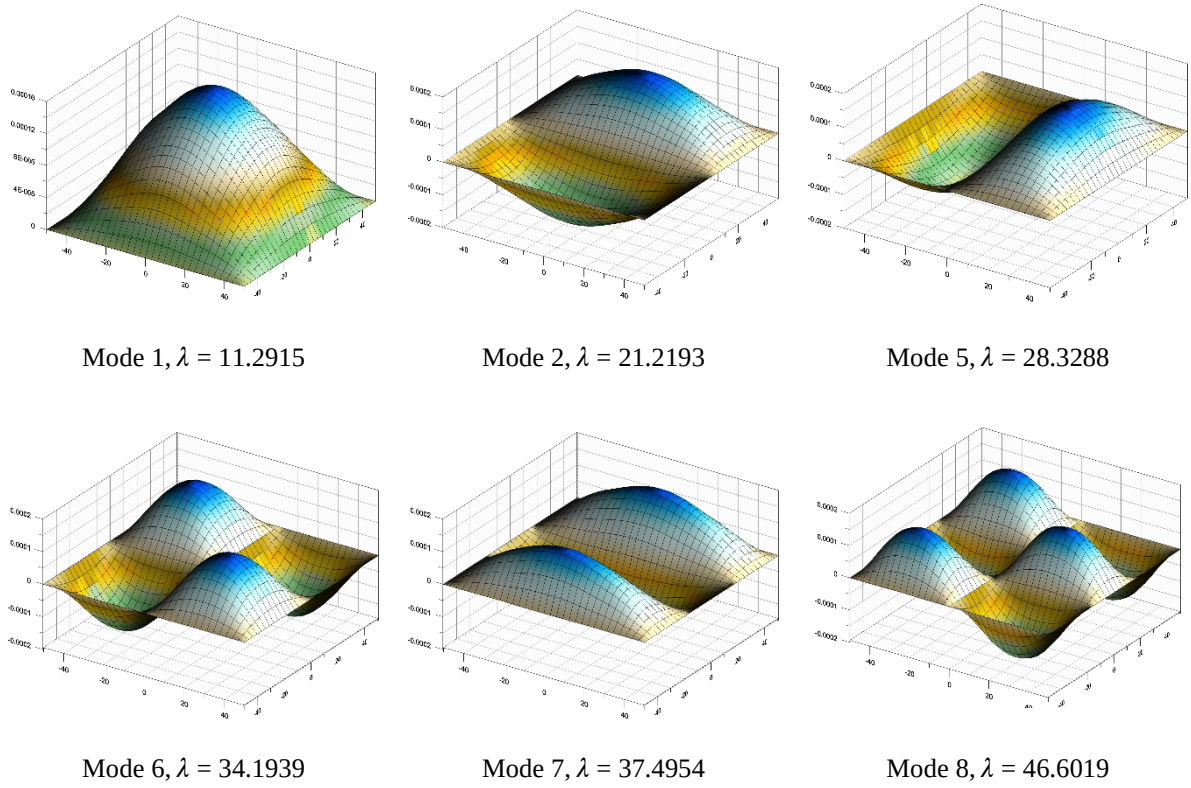

Mode 1, λ = 11.2915 Mode 2, λ = 21.2193 Mode 5, λ = 28.3288

Mode 6, λ = 34.1939 Mode 7, λ = 37.4954 Mode 8, λ = 46.6019

Fig. 2 Selected vibration modes obtained with model **ZZ_1** for simply supported plate, $a = 10\,h$

3.3. Square composite plate with all-round clamped boundary

In the next example the free vibration analysis has been performed for the same graphite-epoxy composite plate (0/90/90/0) as in the previous example, but now the plate is clamped at the edges. The dimensionless frequencies normalized according to (48) are given in Table 4 for three different values of the length to thickness ratio (a/h). The results of the three-dimensional finite element analysis (3D FEA) as provided by Kulkarni & Kapuria [33] have been used as the reference solution.

Table 4. Natural frequencies of clamped (CCCC) square composite (0/90/90/0) plate

a/h	mode	**FSDT_0**		**FSDT_1M**		**FSDT_1R**		**FSDT_3**		**ZZ_1 = ZZ_3**		**ZZ_2**		**3D FEA** [33]
		λ	*Error [%]*	λ	*Error [%]*	λ	*Error [%]*	λ	*Error [%]*	λ	*Error [%]*	λ	*Error [%]*	λ
5	1	12.8730	*12.08*	11.9810	*4.31*	12.0400	*4.82*	10.9205	*-4.92*	11.4592	*-0.23*	11.6856	*1.74*	**11.4860**
	2	19.9014	*8.78*	18.5308	*1.29*	18.6217	*1.78*	17.5204	*-4.24*	18.2021	*-0.51*	18.6979	*2.20*	**18.2956**
	3	21.8339	*12.94*	20.1230	*4.09*	20.2347	*4.67*	17.7433	*-8.22*	19.2791	*-0.27*	19.6533	*1.66*	**19.3319**
	4	26.8090	*10.54*	24.8010	*2.26*	24.9328	*2.81*	22.6211	*-6.72*	24.1466	*-0.43*	24.7146	*1.91*	**24.2519**
	5	29.4901	*7.86*	27.3789	*0.14*	27.5184	*0.65*	25.9017	*-5.26*	27.1758	*-0.60*	28.0164	*2.47*	**27.3411**
	6	32.6013	*12.76*	29.8585	*3.27*	30.0366	*3.89*	26.2090	*-9.35*	28.8015	*-0.38*	29.4207	*1.76*	**28.9117**
	7	34.6477		32.0550		32.2256		29.5606		31.6129		32.4872		
	8	36.2003		33.2732		33.4641		29.9338		32.3812		33.1311		
	9	40.0625		37.0431		37.2420		34.2091		36.9314		38.1557		
	10	42.3713		39.0088		39.2288		35.4980		38.3602		39.3565		
10	1	19.7334	*11.17*	18.7893	*5.85*	18.8535	*6.22*	17.3794	*-2.09*	17.7321	*-0.10*	17.9213	*0.96*	**17.7502**
	2	30.2931	*7.41*	28.9580	*2.68*	29.0497	*3.00*	27.7001	*-1.78*	28.1432	*-0.21*	28.6118	*1.45*	**28.2032**
	3	37.3573	*15.12*	34.8990	*7.55*	35.0619	*8.05*	31.1311	*-4.07*	32.4177	*-0.10*	32.8171	*1.13*	**32.4505**
	4	44.3626	*11.83*	41.7413	*5.22*	41.9165	*5.66*	38.3265	*-3.39*	39.5891	*-0.20*	40.1782	*1.28*	**39.6697**
	5	46.6503	*6.62*	44.3475	*1.36*	44.5048	*1.72*	42.8870	*-1.98*	43.6058	*-0.33*	44.5835	*1.90*	**43.7521**
	6	57.1973	*13.36*	53.9287	*6.88*	54.1486	*7.32*	47.7378	*-5.39*	50.4004	*-0.11*	51.0903	*1.26*	**50.4570**
	7	58.5988		54.3058		54.5880		50.7220		52.1275		53.1505		
	8	63.5733		59.1979		59.4868		52.9777		55.5646		56.3848		
	9	66.0450		62.3657		62.6147		60.4474		61.5688		63.1985		
	10	73.3649		68.5602		68.8793		62.7322		65.3519		66.5152		
20	1	25.1742	*6.13*	24.6049	*3.73*	24.6452	*3.90*	23.5784	*-0.60*	23.7103	*-0.05*	23.8225	*0.43*	**23.7212**
	2	37.7470	*3.94*	37.0160	*1.93*	37.0680	*2.07*	36.1099	*-0.57*	36.2849	*-0.08*	36.5265	*0.58*	**36.3153**
	3	55.1367	*11.15*	52.8801	*6.60*	53.0360	*6.91*	48.9095	*-1.40*	49.5851	*-0.04*	49.9519	*0.70*	**49.6061**
	4	60.2497	*4.47*	58.9004	*2.13*	58.9963	*2.30*	56.9457	*-1.26*	57.6213	*-0.09*	58.0650	*0.68*	**57.6707**
	5	62.9390	*8.04*	60.6492	*4.10*	60.8076	*4.38*	57.8675	*-0.67*	58.1922	*-0.11*	58.7909	*0.91*	**58.2579**
	6	79.6068	*6.92*	76.9878	*3.40*	77.1699	*3.64*	73.5913	*-1.16*	74.3569	*-0.14*	75.0794	*0.83*	**74.4577**
	7	89.7996		87.2758		87.4539		80.0812		81.7878		82.5324		
	8	93.2220		88.3227		88.6550		85.6654		86.3827		87.5857		
	9	98.7306		93.8346		94.1667		85.9957		87.5433		88.3519		
	10	104.6949		101.1810		101.4260		97.8054		98.8037		100.0839		

By examining the numbers given in Table 4, one can see that the clamped boundary conditions turned out to be more demanding for the FOSD models, the behavior of which cannot be considered satisfactory, perhaps with the exception of the **FOSD_3** model, but only for the thinnest plate under consideration ($a = 20\,h$). One should remember that the global shear correction proposed by Rolfes & Rohwer [22] was constructed assuming a cylindrical deformation profile, which, however, differs significantly from that of the clamped plate. The three models based on the zig-zag functions can provide satisfactory solutions for all three aspect ratios considered, but here, again, the best accuracy can be obtained when the zig-zag deformation profile is enhanced by the RMVT formulation ensuring continuity of interlaminar shear stress (models **ZZ_1** and **ZZ_3**).

The vibration modes for the clamped plate followed a predictable and quite regular scheme as can be observed in Fig. 3.

3.4. Clamped square sandwich plate (0/90/Core/90/0)

Kulkarni & Kapuria [33] provided the results of the three-dimensional fine mesh ABAQUS analysis of natural vibrations for different variants of sandwich panels with faces made as fiber reinforced composite laminates. These results can serve as an excellent reference solution for benchmarking other models. The problem discussed in this section relates to a sandwich panel consisted of an orthotropic glass fiber honeycomb core and two thin face-sheets each made as 2-layer cross-ply (90/0) graphite-epoxy composite. Such a structure can be also described as a five-layer (0/90/Core/90/0) laminate. The thickness of the central core is taken as $0.8\,h$, while that of each graphite-epoxy ply is $0.05\,h$. The material parameters are given in Table 5.

Table 5. Material parameters for sandwich plate

	ρ [kg/m^3]	E_a [GPa]	E_b [GPa]	G_{ab} [GPa]	G_{ac} [GPa]	G_{bc} [GPa]	ν_{ab}
graphite-epoxy faces	681.8	276	6.9	6.9	6.9	6.9	0.25
honeycomb core	1000	0.5776	0.5776	0.1079	0.1079	0.22215	0.0025

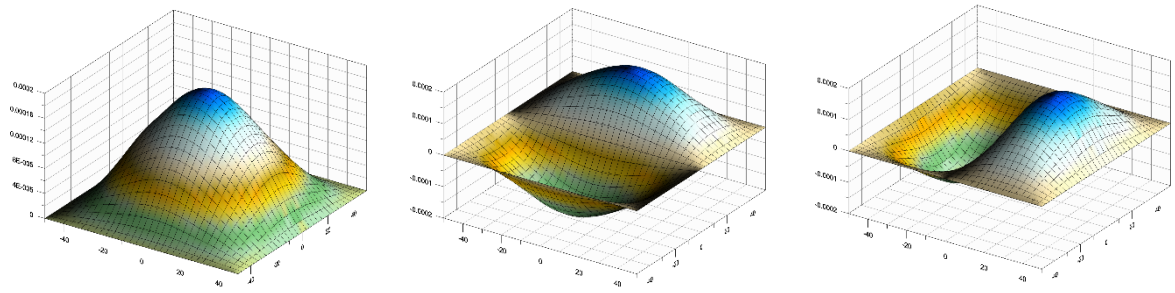

Mode 1, λ = 17.7321 Mode 2, λ = 28.1432 Mode 3, λ = 32.4177

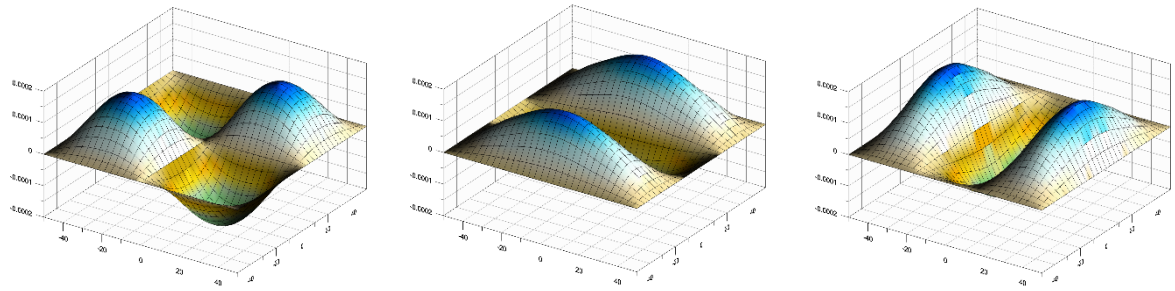

Mode 4, λ = 39.5891 Mode 5, λ = 43.6058 Mode 6, λ = 50.4004

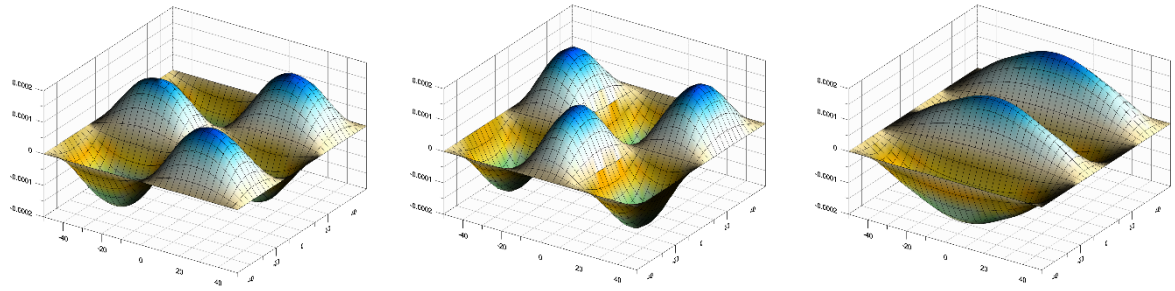

Mode 7, λ = 52.1275 Mode 8, λ = 55.5646 Mode 9, λ = 61.5688

Fig. 3. The first 9 vibration modes calculated with model **ZZ_3** for clamped composite plate $a = 10\,h$

Estimations of the first six natural frequencies calculated with the examined ESL models for three different values of the length to thickness ratio (a/h) have been confronted with the 3D FEA results provided by Kulkarni & Kapuria [33] applying the following normalization:

$$\lambda = 100\,\omega\,a\sqrt{\frac{\rho_{(core)}}{E_{a(core)}}}\,. \tag{49}$$

The error rates of own solutions are listed in Table 6.

Table 6. Accuracy of ESL models for clamped (CCCC) square sandwich plate (0/90/Core/90/0)

a/h	Mode	**3D FEA** [33] $\boldsymbol{\lambda}$	**FOSD_0** *Error [%]*	**FOSD_1M** *Error [%]*	**FOSD_1R** *Error [%]*	**FOSD_3** *Error [%]*	**ZZ_1** *Error [%]*	**ZZ_2** *Error [%]*	**ZZ_3** *Error [%]*
5	1	**12.0464**	*165.86*	*143.56*	*145.01*	*-8.49*	*153.77*	*0.84*	*0.76*
	2	**18.2701**	*175.28*	*151.86*	*153.38*	*-12.00*	*162.26*	*0.92*	*0.82*
	3	**20.5724**	*147.01*	*126.19*	*127.54*	*-9.39*	*135.98*	*0.99*	*0.91*
	4	**24.8738**	*157.92*	*135.99*	*137.41*	*-11.43*	*146.01*	*1.00*	*0.90*
	5	**26.4054**	*175.65*	*151.31*	*152.88*	*-16.21*	*161.98*	*1.30*	*1.15*
	6	**30.6442**	*141.95*	*120.78*	*122.15*	*-12.62*	*130.81*	*1.20*	*1.10*
10	1	**11.2236**	*146.99*	*130.99*	*132.06*	*-3.86*	*138.42*	*0.53*	*0.48*
	2	**16.6777**	*171.38*	*151.43*	*152.74*	*-5.31*	*160.33*	*0.53*	*0.47*
	3	**18.9650**	*139.33*	*122.11*	*123.24*	*-4.22*	*130.29*	*0.65*	*0.59*
	4	**22.7096**	*155.66*	*136.61*	*137.86*	*-5.00*	*145.38*	*0.61*	*0.55*
	5	**23.5270**	*187.82*	*165.09*	*166.57*	*-6.84*	*175.11*	*0.54*	*0.48*
	6	**28.0728**	*143.17*	*124.43*	*125.65*	*-5.89*	*133.38*	*0.68*	*0.62*
20	1	**10.1635**	*92.92*	*86.34*	*86.80*	*-1.61*	*89.46*	*0.61*	*0.57*
	2	**15.2734**	*128.21*	*117.68*	*118.40*	*-2.42*	*122.82*	*0.71*	*0.66*
	3	**17.2645**	*106.16*	*95.74*	*96.45*	*-1.91*	*100.46*	*0.85*	*0.79*
	4	**20.7882**	*121.73*	*110.33*	*111.11*	*-2.26*	*115.67*	*0.82*	*0.76*
	5	**21.8260**	*155.52*	*141.01*	*141.98*	*-2.91*	*148.07*	*0.71*	*0.66*
	6	**26.0346**	*117.75*	*104.43*	*105.32*	*-2.66*	*110.36*	*0.78*	*0.73*

Even a quick glance at the results presented in Table 6 shows that most of the tested models were not able to provide a satisfactory estimation of the natural frequency for the clamped five-layer (0/90/Core/90/0) plate. The error values for four models (**FOSD_0**, **FOSD_1M**, **FOSD_1R** and **ZZ_01**) even exceeded 100 percent. It is true that the application of the global transverse shear correction in the **FOSD_3** model significantly improved the accuracy of the solution, but only the results for the thinnest of the analyzed plates ($a = 20\ h$) can be considered satisfactory. The low accuracy of the model **ZZ_01** may be also a negative surprise; however, it should be noted that this formulation does not take into account the relatively large difference in stiffness of the core and the faces. Since this difference is included in the Tessler zigzag function (19), both models in which it was used (**ZZ_2** and **ZZ_3**) were able to provide very good accuracy of solutions. It may be interesting that the same example of the clamped five-layer (0/90/Core/90/0) plate was analyzed in [36] with the Refined Zigzag Theory based also

on the function (19); however, the accuracy of the results presented in [36] was lower than that obtained with the use of the **ZZ_2** and **ZZ_3** models.

3.5. Clamped-free (CFCF) square sandwich plate (0/90/Core/90/0)

Another interesting example from the collection of problems with the 3D FEA results provided by Kulkarni & Kapuria [33] is the same square sandwich plate (0/90/Core/90/0), as analyzed in the previous example but with modified boundary conditions - now the plate is clamped at two opposite edges, and the other two remain free (CFCF).

Table 7 presents the assessment of the accuracy of own results in terms of the first six frequencies of flexural free vibrations tin relation to the FEA 3D results [33].

Table 7. Accuracy of ESL models for clamped-free (CFCF) square sandwich plate (0/90/Core/90/0)

a/h	Mode	**3D FEA** [33] $\boldsymbol{\lambda}$	**FOSD_0** *Error [%]*	**FOSD_1M** *Error [%]*	**FOSD_1R** *Error [%]*	**FOSD_3** *Error [%]*	**ZZ_1** *Error [%]*	**ZZ_2** *Error [%]*	**ZZ_3** *Error [%]*
5	1	**7.5449**	*197.59*	*172.32*	*173.96*	*-10.34*	*183.33*	*0.74*	*0.66*
	2	**9.2411**	*152.07*	*132.35*	*133.63*	*-6.01*	*140.93*	*0.54*	*0.48*
	3	**15.5981**	*186.66*	*162.16*	*163.75*	*-13.38*	*172.82*	*0.92*	*0.81*
	4	**17.3404**	*158.61*	*141.38*	*142.53*	*-10.92*	*149.52*	*0.76*	*0.68*
	5	**18.9511**	*141.96*	*124.31*	*125.59*	*-3.59*	*132.89*	*0.37*	*0.34*
	6	**23.5989**	*95.93*	*94.31*	*94.31*	*-13.82*	*94.31*	*0.56*	*0.50*
10	1	**7.0119**	*180.70*	*161.88*	*163.14*	*-4.80*	*170.22*	*0.45*	*0.40*
	2	**7.7131**	*161.12*	*144.03*	*145.17*	*-3.33*	*151.60*	*0.40*	*0.36*
	3	**14.1496**	*137.50*	*127.04*	*127.75*	*-6.00*	*131.93*	*0.50*	*0.45*
	4	**15.1975**	*167.57*	*147.27*	*148.60*	*-4.90*	*156.16*	*0.45*	*0.40*
	5	**17.0942**	*142.30*	*124.42*	*125.59*	*-1.28*	*132.25*	*0.14*	*0.12*
	6	**21.3089**	*115.19*	*115.19*	*115.19*	*-5.23*	*115.19*	*0.26*	*0.23*
20	1	**6.4836**	*118.29*	*110.40*	*110.95*	*-2.09*	*113.99*	*0.59*	*0.55*
	2	**6.7496**	*114.44*	*106.69*	*107.23*	*-1.71*	*110.22*	*0.58*	*0.54*
	3	**13.0570**	*64.08*	*60.14*	*60.41*	*-2.81*	*61.97*	*0.74*	*0.69*
	4	**13.5350**	*141.56*	*128.62*	*129.50*	*-2.42*	*134.41*	*0.70*	*0.65*
	5	**13.6626**	*142.39*	*129.54*	*130.41*	*-0.50*	*135.29*	*0.17*	*0.16*
	6	**18.1674**	*105.58*	*96.16*	*96.80*	*-1.38*	*100.40*	*0.41*	*0.38*

It should be noted that the boundary conditions adopted in this example do not eliminate the in-plane vibration modes. The vibration frequency corresponding to such a form of vibration could be easily identified in the results of own calculations because its normalized value λ (49)

was equal to 22.9555 for all three considered plate thicknesses regardless of the choice of the calculation model. However, because the set of results of the 3D FEM analysis presented in [33] does not include in-plane modes, therefore, for the sake of clearer presentation, only the out-of-plane vibrations have been included in Table 7.

From the results shown in Table 7, almost exactly the same conclusions can be drawn as in the analysis of the results of the previous example. The modification of boundary conditions did not change much here. It is worth noting, however, that the analysis of the obtained values of natural frequencies alone is usually not sufficient to evaluate the computational models. It should be remembered that with different computational models it is also possible to obtain a different order of vibration modes.

The flexural vibration modes established with application of model **ZZ_3** for the square CFCF sandwich plate $a = 5\,h$ are illustrated in Figure 4.

4. Final conclusions

The performance of seven various ESL models in a natural vibration FEA of multi-layered plates has been examined in the paper. The four variants of the classical FOSD formulation diversified by an application of different transverse shear correction were accompanied by three models refined by the application of the zig-zag functions. The comparative examination of the selected models has been performed for the variety of benchmark examples with available reference solutions, either exact analytical 3D elastic or 3D FEA, for free vibration analysis of multi-layered plates with various support conditions.

The difference in the values of the shear correction coefficients in Reissner's ($\kappa = 5/6$) and Mindlin's ($\kappa = \pi^2/12$) variants is slightly above 1 percent, but the use of the latter variant usually allows for a better estimation of the fundamental frequency of free vibrations of moderately thick isotropic plates. However, in the cases of multi-layered plates examined in this study, it

was difficult to observe a similar advantage of the **FOSD_1M** model over the **FOSD_1R** one, as, generally, both those approaches do not account for the layered structure of the plate and ignore stiffness differences among individual layers. The concept of global transverse shear correction applied in model **FOSD_3** offered a better accuracy of calculations; nevertheless, it did not work as good as in static applications which should not come as a surprise given the static nature of the compounds from which this concept is derived. It should also be noted that the efficiency of the model **FOSD_3** strongly depends on the support conditions; for freely supported slabs, the solutions obtained with this model offered an accuracy similar to that obtained with the use of models based on zig-zag functions.

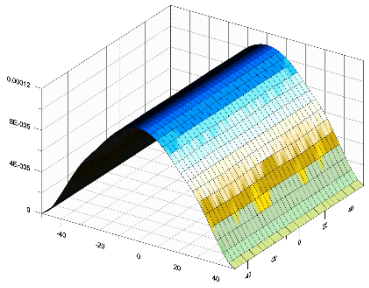

Mode 1, λ = 7.5946

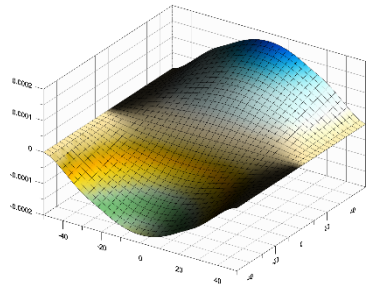

Mode 2, λ = 9.2858

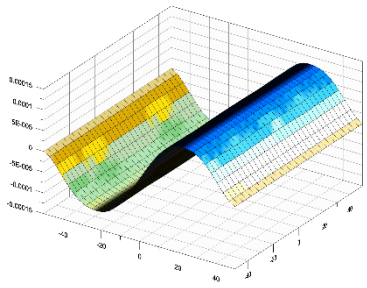

Mode 3, λ = 15.7246

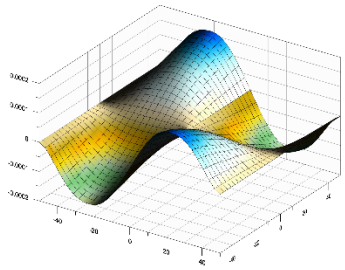

Mode 4, λ = 17.4575

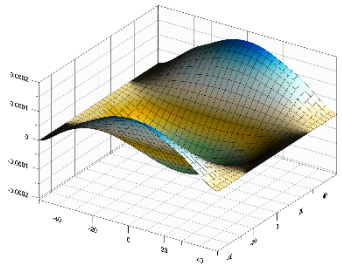

Mode 5, λ = 19.0157

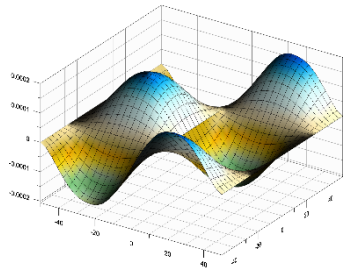

Mode 7, λ = 23.7178

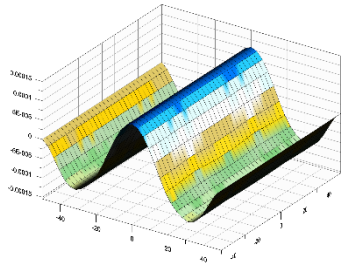

Mode 8, λ = 24.8592

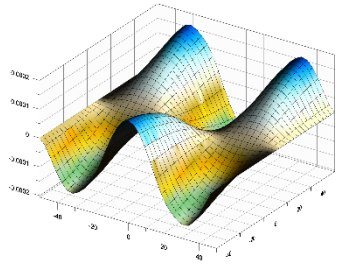

Mode 9, λ = 26.2555

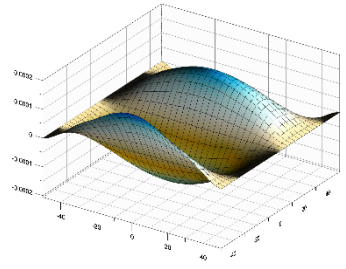

Mode 10, λ = 27.4899

Fig. 4. The first 9 flexural vibration modes calculated with model **ZZ_3** for CFCF sandwich plate $a = 5\ h$

It came as no surprise that computational models based on zig-zag functions performed generally better than the FOSD models. In most of the analyzed cases, it was also possible to notice the advantage of models **ZZ_1** and **ZZ_3** based on the RMVT formulation ensuring the continuity of the interlayer shear stress over the **ZZ_2** approach built of PVD, in which these continuity conditions were not met. However, in the last two examples it turned out that the **ZZ_1** model utilizing the Murakami function (17) which simulates the zig-zag effect in an arbitrary manner without considering the material stiffness, failed when there was a large difference in shear stiffness between the layers. It was surprising that even the **FOSD_1M** and **FOSD_1R** models performed better in these examples than the **ZZ_1** one. Taking into account all the presented results, it should be noted that the **ZZ_3** model offered the best accuracy among all the tested models.

Finally, it seems reasonable to point out that in similar comparative analyzes as carried out in this report, one cannot limit oneself only to determining the value of the frequency of vibrations, because depending on the adopted calculation model, there may be shifts in the order of vibration modes.

LITERATURE

1. Mindlin, R. D. (1951). Influence of Rotatory Inertia and Shear on Flexural Motions of Isotropic, Elastic Plates. *Journal of Applied Mechanics, Transactions ASME*, 18, 31–38. https://doi.org/10.1007/978-1-4613-8865-4_29
2. Reissner, E. (1944). On the Theory of Bending of Elastic Plates. *Journal of Mathematics and Physics*, 23(1–4), 184–191. https://doi.org/10.1002/sapm1944231184
3. Reissner, E. (1945) The Effect of Transverse Shear Deformation on the Bending of Elastic Plates. *Journal of Applied Mechanics* 12: A69-A77
4. Hencky, H. (1947). Über die Berücksichtigung der Schubverzerrung in ebenen Platten. *Ingenieur-Archiv*, 16(1), 72–76. https://doi.org/10.1007/BF00534518
5. Reissner, E. (1985). Reflections on the Theory of Elastic Plates. *Applied Mechanics Reviews*, 38(11), 1453–1464. https://doi.org/10.1115/1.3143699
6. Ramm, E. (2000). From Reissner Plate Theory to Three Dimensions in Large Deformation Shell Analysis. *ZAMM*, 80(1), 61–68. https://doi.org/10.1002/(SICI)1521-4001(200001)80:1<61::AID-ZAMM61>3.0.CO;2-E
7. Timoshenko, S. P. (1921). LXVI. On the correction for shear of the differential equation for transverse vibrations of prismatic bars. *The London, Edinburgh, and Dublin Philosophical Magazine and Journal of Science*, 41(245), 744–746. https://doi.org/10.1080/14786442108636264
8. Yang, P. C., Norris, C. H., & Stavsky, Y. (1966). Elastic wave propagation in heterogeneous plates. *International Journal of Solids and Structures*, *2*(4), 665–684. https://doi.org/10.1016/0020-7683(66)90045-X
9. Jones, R. M (1999). *Mechanics of Composite Materials* (2nd ed.). Boca Raton: CRC Press, https://doi.org/10.1201/9781498711067

10. Reddy JN (2004) *Mechanics of Laminated Composite Plates and Shells: Theory and Analysis*, Second Ed. CRC Press, Philadelphia
11. Kreja, I. (2011). A literature review on computational models for laminated composite and sandwich panels. *Open Engineering* (Formerly *Central European Journal of Engineering*), 1(1), 1–39. https://doi.org/10.2478/s13531-011-0005-x
12. Chow, T. S. (1971). On the Propagation of Flexural Waves in an Orthotropic Laminated Plate and Its Response to an Impulsive Load. *Journal of Composite Materials*, *5*(3), 306–319. https://doi.org/10.1177/002199837100500302
13. Whitney, J. M. (1973). Shear Correction Factors for Orthotropic Laminates under Static Load. *Journal of Applied Mechanics*, *40*(1), 302–304. https://doi.org/10.1115/1.3422950
14. Reddy, J. N. (1984). A simple higher-order theory for laminated composite plates. *Journal of Applied Mechanics, Transactions ASME*, 51(4), 745–752. https://doi.org/10.1115/1.3167719
15. Carrera, E. (2003). Historical review of Zig-Zag theories for multilayered plates and shells. *Applied Mechanics Reviews*, *56*(3), 287–308. https://doi.org/10.1115/1.1557614
16. Ambartsumyan, S. A. (1970). *Theory of anisotropic plates: strength, stability, vibration*. Stamford, Conn.: Technomic Publishing Co., Inc.,.
17. Murakami, H. (1986). Laminated composite plate theory with improved in-plane responses. *Journal of Applied Mechanics, Transactions ASME*, 53(3), 661–666. https://doi.org/10.1115/1.3171828
18. Reddy, J. N. (1987). Generalization of Two-Dimensional Theories of Laminated Composite Plates. *Communications in Applied Numerical Methods*, *3*(3), 173–180. https://doi.org/10.1002/cnm.1630030303
19. Carrera, E. (2000). An assessment of mixed and classical theories on global and local response of multilayered orthotropic plates. *Composite Structures*, *50*(2), 183–198. https://doi.org/10.1016/S0263-8223(00)00099-4
20. Zappino, E., Li, G., Pagani, A., & Carrera, E. (2017). Global-local analysis of laminated plates by node-dependent kinematic finite elements with variable ESL/LW capabilities. *Composite Structures*, *172*, 1–14. https://doi.org/10.1016/j.compstruct.2017.03.057
21. Kreja, I., & Sabik, A. (2019). Equivalent single-layer models in deformation analysis of laminated multilayered plates. *Acta Mechanica*, 230(8), 2827–2851. https://doi.org/10.1007/s00707-019-02434-7
22. Rolfes, R., & Rohwer, K. (1997). Improved transverse shear stresses in composite finite elements based on first order shear deformation theory. *International Journal for Numerical Methods in Engineering*, *40*(1), 51–60. https://doi.org/10.1002/(SICI)1097-0207(19970115)40:1<51::AID-NME49>3.0.CO;2-3
23. Tessler, A., Di Sciuva, M., & Gherlone, M. (2010). A consistent refinement of first-order shear deformation theory for laminated composite and sandwich plates using improved zigzag kinematics. *Journal of Mechanics of Materials and Structures*, *5*(2), 341–367. https://doi.org/10.2140/jomms.2010.5.341
24. Reissner, E. (1984). On a certain mixed variational theorem and a proposed application. *International Journal for Numerical Methods in Engineering*, *20*(7), 1366–1368. https://doi.org/10.1002/nme.1620200714
25. Carrera, E. (1996). C0 Reissner-Mindlin Multilayered Plate Elements Including Zig-Zag And Interlaminar Stress Continuity. *International Journal for Numerical Methods in Engineering*, *39*(11), 1797–1820. https://doi.org/10.1002/(SICI)1097-0207(19960615)39:11<1797::AID-NME928>3.0.CO;2-W
26. Sabik, A., & Kreja, I. (2008). Linear analysis of laminated multilayered plates with the application of zig-zag function. *Archives of Civil and Mechanical Engineering*, *8*(4), 61–72. https://doi.org/10.1016/S1644-9665(12)60122-8
27. Srinivas, S., Joga Rao, C. V., & Rao, A. K. (1970). An exact analysis for vibration of simply-supported homogeneous and laminated thick rectangular plates. *Journal of Sound and Vibration*, *12*(2), 187–199. https://doi.org/10.1016/0022-460X(70)90089-1
28. Srinivas, S., & Rao, A. K. (1970). Bending, vibration and buckling of simply supported thick orthotropic rectangular plates and laminates. *International Journal of Solids and Structures*, *6*(11), 1463–1481. https://doi.org/10.1016/0020-7683(70)90076-4
29. Noor, A. K. (1973). Free vibrations of multilayered composite plates. *AIAA Journal*, *11*(7), 1038–1039. https://doi.org/10.2514/3.6868
30. Reddy, J. N., & Kuppusamy, T. (1984). Natural vibrations of laminated anisotropic plates. *Journal of Sound and Vibration*, *94*(1), 63–69. https://doi.org/10.1016/S0022-460X(84)80005-X
31. Noor, A. K., & Burton, W. S. (1989). Stress and free vibration analyses of multilayered composite plates. *Composite Structures*, *11*(3), 183–204. https://doi.org/10.1016/0263-8223(89)90058-5
32. Noor, A. K., & Burton, W. S. (1990). Three-dimensional solutions for antisymmetrically laminated anisotropic plates. *Journal of Applied Mechanics, Transactions ASME*, *57*(1), 182–188. https://doi.org/10.1115/1.2888300
33. Kulkarni, S. D., & Kapuria, S. (2008). Free vibration analysis of composite and sandwich plates using an improved discrete Kirchhoff quadrilateral element based on third-order zigzag theory. *Computational Mechanics*, *42*(6), 803–824. https://doi.org/10.1007/s00466-008-0285-z
34. Kreja, I., Schmidt, R., & Reddy, J. N. (1997). Finite elements based on a first-order shear deformation moderate rotation shell theory with applications to the analysis of composite structures. *International Journal*

of Non-Linear Mechanics, 32(6), 1123–1142. https://doi.org/http://dx.doi.org/10.1016/S0020-7462(96)00124-2
35. Bathe, K.-J. (1996) *Finite Element Procedures*, Prentice-Hall Inc., Englewood Cliffs, NJ, 1996.
36. Iurlaro, L., Gherlone, M., Di Sciuva, M., & Tessler, A. (2013). Assessment of the Refined Zigzag Theory for bending, vibration, and buckling of sandwich plates: A comparative study of different theories. *Composite Structures*, *106*, 777–792. https://doi.org/10.1016/j.compstruct.2013.07.019

Appendix A

Formulas for the inertia components introduced in (37):

$$I_0 = \sum_{k=1}^{N}\left(\int_{z_{(k-1)}}^{z_k} \rho dz\right) = \sum_{k=1}^{N}\left(\rho_k h_k\right)$$

$$I_1 = \sum_{k=1}^{N}\left(\int_{z_{(k-1)}}^{z_k} z\rho dz\right) = \sum_{k=1}^{N}\left(\rho_k \frac{\left(z_k\right)^2 - \left(z_{(k-1)}\right)^2}{2}\right)$$

$$I_2 = \sum_{k=1}^{N}\left(\int_{z_{(k-1)}}^{z_k} z^2\rho dz\right) = \sum_{k=1}^{N}\left(\rho_k \frac{\left(z_k\right)^3 - \left(z_{(k-1)}\right)^3}{3}\right)$$

$$J_{x0}^1 = \sum_{k=1}^{N}\left(\int_{z_{(k-1)}}^{z_k} \rho\phi_x^{(k)}(z)dz\right) = \sum_{k=1}^{N}\left(\rho_k \int_{z_{(k-1)}}^{z_k} \phi_x^{(k)}(z)dz\right)$$

$$J_{y0}^1 = \sum_{k=1}^{N}\left(\int_{z_{(k-1)}}^{z_k} \rho\phi_y^{(k)}(z)dz\right) = \sum_{k=1}^{N}\left(\rho_k \int_{z_{(k-1)}}^{z_k} \phi_y^{(k)}(z)dz\right)$$

$$J_{x1}^1 = \sum_{k=1}^{N}\left(\int_{z_{(k-1)}}^{z_k} \rho z\phi_x^{(k)}(z)dz\right) = \sum_{k=1}^{N}\left(\rho_k \int_{z_{(k-1)}}^{z_k} z\phi_x^{(k)}(z)dz\right)$$

$$J_{y1}^1 = \sum_{k=1}^{N}\left(\int_{z_{(k-1)}}^{z_k} \rho z\phi_y^{(k)}(z)dz\right) = \sum_{k=1}^{N}\left(\rho_k \int_{z_{(k-1)}}^{z_k} z\phi_y^{(k)}(z)dz\right)$$

$$J_{x0}^2 = \sum_{k=1}^{N}\left(\int_{z_{(k-1)}}^{z_k} \rho\left(\phi_x^{(k)}(z)\right)^2 dz\right) = \sum_{k=1}^{N}\left(\rho_k \int_{z_{(k-1)}}^{z_k} \left(\phi_x^{(k)}(z)\right)^2 dz\right).$$

$$J_{y0}^2 = \sum_{k=1}^{N}\left(\int_{z_{(k-1)}}^{z_k} \rho\left(\phi_y^{(k)}(z)\right)^2 dz\right) = \sum_{k=1}^{N}\left(\rho_k \int_{z_{(k-1)}}^{z_k} \left(\phi_y^{(k)}(z)\right)^2 dz\right)$$

Appendix B

The global transverse shear stiffness for the **FOSD_3** model is calculated following the proposal of Rolfes & Rohwer [22] starting with the idea that transverse shear stresses can be obtained from the equilibrium equations:

$$\begin{aligned} \sigma_{xx},_x + \sigma_{yx},_y + \sigma_{zx},_z + f_x = 0 \\ \sigma_{xy},_x + \sigma_{yy},_y + \sigma_{zy},_z + f_y = 0 \end{aligned} \tag{B.1}$$

with f_x and f_y standing for the appropriate components of body forces. In the absence of body forces one would obtain:

$$\begin{aligned} \sigma_{xz}(z) = -\int_{-\frac{h}{2}}^{z} \left(\sigma_{xx},_x + \sigma_{xy},_y \right) d\bar{z} \\ \sigma_{yz}(z) = -\int_{-\frac{h}{2}}^{z} \left(\sigma_{xy},_x + \sigma_{yy},_y \right) d\bar{z}. \end{aligned} \tag{B.2}$$

By analogy to (8) the membrane forces and bending moments can be acquired by the through-the-thickness integration of the appropriate stress components:

$$\begin{aligned} N_{xx} = \int_{-\frac{h}{2}}^{\frac{h}{2}} \sigma_{xx}\, dz, \quad N_{yy} = \int_{-\frac{h}{2}}^{\frac{h}{2}} \sigma_{yy}\, dz, \quad N_{xy} = \int_{-\frac{h}{2}}^{\frac{h}{2}} \sigma_{xy}\, dz, \\ M_{xx} = \int_{-\frac{h}{2}}^{\frac{h}{2}} z\, \sigma_{xx}\, dz, \quad M_{yy} = \int_{-\frac{h}{2}}^{\frac{h}{2}} z\, \sigma_{yy}\, dz, \quad M_{xy} = \int_{-\frac{h}{2}}^{\frac{h}{2}} z\, \sigma_{xy}\, dz. \end{aligned} \tag{B.3))}$$

In the FOSD formulation, the in-plane strain components for a plate can be presented as

$$\left\{ \boldsymbol{\varepsilon}_B(x,\, y,\, z) \right\} = \begin{Bmatrix} \varepsilon_{xx}(x,\, y,\, z) \\ \varepsilon_{yy}(x,\, y,\, z) \\ \gamma_{xy}(x,\, y,\, z) \end{Bmatrix} = \left\{ \varepsilon_0 \right\} + z \left\{ \kappa \right\} \tag{B.4}$$

with

$$\left\{ \varepsilon_0 \right\} = \begin{Bmatrix} \varepsilon_{x0}(x,\, y) \\ \varepsilon_{y0}(x,\, y) \\ \gamma_{xy0}(x,\, y) \end{Bmatrix}, \quad \left\{ \kappa \right\} = \begin{Bmatrix} \kappa_x(x,\, y) \\ \kappa_y(x,\, y) \\ \kappa_{xy}(x,\, y) \end{Bmatrix}, \tag{B.5}$$

$$\varepsilon_{x0}(x,\,y)=\frac{\partial u(x,\,y)}{\partial x},\quad \varepsilon_{y0}(x,\,y)=\frac{\partial v(x,\,y)}{\partial y},$$
$$\gamma_{xy0}(x,\,y)=\frac{\partial u(x,\,y)}{\partial y}+\frac{\partial v(x,\,y)}{\partial x},\quad \kappa_{x}(x,\,y)=\frac{\partial \varphi_{x}(x,\,y)}{\partial x},\tag{B.6}$$
$$\kappa_{y}(x,\,y)=\frac{\partial \varphi_{y}(x,\,y)}{\partial y},\quad \kappa_{xy}(x,\,y)=\frac{\partial \varphi_{x}(x,\,y)}{\partial y}+\frac{\partial \varphi_{y}(x,\,y)}{\partial x}.$$

After introducing the following substitutions ($\{N\}$ should be distinguished from [**N**] standing for the shape functions matrix, and $\{M\}$ should not be mistaken with [**M**] introduced earlier to represent the mass matrix):

$$\{N\}=\begin{Bmatrix}N_{xx}\\N_{yy}\\N_{xy}\end{Bmatrix},\quad \{M\}=\begin{Bmatrix}M_{xx}\\M_{yy}\\M_{xy}\end{Bmatrix},\tag{B.7}$$

the following constitutive relation can be presented

$$\begin{Bmatrix}\{N\}\\\{M\}\end{Bmatrix}=\begin{bmatrix}[A] & [B]\\[B] & [D]\end{bmatrix}\begin{Bmatrix}\{\varepsilon_0\}\\\{\kappa\}\end{Bmatrix}\tag{B.8}$$

with

$$[A]=\begin{bmatrix}a_{11} & a_{12} & a_{13}\\a_{12} & a_{22} & a_{23}\\a_{13} & a_{23} & a_{33}\end{bmatrix},\quad a_{ij}=\int_{-\frac{h}{2}}^{\frac{h}{2}}c_{ij}\;dz,\tag{B.9}$$

$$[B]=\begin{bmatrix}b_{11} & b_{12} & b_{13}\\b_{12} & b_{22} & b_{23}\\b_{13} & b_{23} & b_{33}\end{bmatrix},\qquad b_{ij}=\int_{-\frac{h}{2}}^{\frac{h}{2}}z\,c_{ij}\;dz,\tag{B.10}$$

$$[D]=\begin{bmatrix}d_{11} & d_{12} & d_{13}\\d_{12} & d_{22} & d_{23}\\d_{13} & d_{23} & d_{33}\end{bmatrix},\qquad d_{ij}=\int_{-\frac{h}{2}}^{\frac{h}{2}}z^2\,c_{ij}\;dz.\tag{B.11}$$

Rolfes & Rohwer [22] suggested that the influence of membrane forces $\{N\}$ on the transverse shear stresses could be ignored what resulted in

$$\{\varepsilon_0\}=-[A]^{-1}[B]\{\kappa\}\tag{B.12}$$

and consequently

$$\{M\} = \underbrace{\left([D]-[B][A]^{-1}[B]\right)}_{[D^*]}\{\kappa\} \tag{B.13}$$

With (B.4) and (6) the formula (B.2) can be transferred to

$$\{\boldsymbol{\sigma}_S(z)\} = -\int_{-\frac{h}{2}}^{z}\left([b_1][\mathbf{C}_B]\left(\{\varepsilon_{0,x}\}+\overline{z}\{\kappa_{,x}\}\right)+[b_2][\mathbf{C}_B]\left(\{\varepsilon_{0,y}\}+\overline{z}\{\kappa_{,y}\}\right)\right)d\overline{z} \tag{B.14}$$

where two Boolean matrices were introduced:

$$[b_1]=\begin{bmatrix}1 & 0 & 0\\ 0 & 0 & 1\end{bmatrix},\quad [b_2]=\begin{bmatrix}0 & 0 & 1\\ 0 & 1 & 0\end{bmatrix}. \tag{B.15}$$

Next by using (B.12) and (B.13) in (B.14) one can arrive at

$$\{\boldsymbol{\sigma}_S(z)\} = -[b_1][F(z)]\{M_{,x}\}-[b_2][F(z)]\{M_{,y}\}, \tag{B.16}$$

with the following substitution:

$$[F(z)]=\int_{-\frac{h}{2}}^{z}\left([\mathbf{C}_B]\left(z-[A]^{-1}[B]\right)\right)d\overline{z}\,[D^*]^{-1}. \tag{B.17}$$

Further considerations require the use of the cylindrical bending assumption; then by utilizing the differential relation between the resulting transverse shear forces and bending moments separately for x and y directions one can adopt the following relations:

$$\{M_{,x}\}=\begin{Bmatrix}M_{x,x}\\ 0\\ 0\end{Bmatrix}=\begin{Bmatrix}-T_{xz}\\ 0\\ 0\end{Bmatrix},\quad \{M_{,y}\}=\begin{Bmatrix}0\\ M_{y,y}\\ 0\end{Bmatrix}=\begin{Bmatrix}0\\ -T_{yz}\\ 0\end{Bmatrix}. \tag{B.18}$$

With (B.16) and (B.18) one can arrive at the following relation between transverse shear stresses and the resulting transverse shear forces:

$$\begin{Bmatrix}\sigma_{xz}(z)\\ \sigma_{yz}(z)\end{Bmatrix}=\begin{bmatrix}F_{11}(z) & F_{32}(z)\\ F_{31}(z) & F_{22}(z)\end{bmatrix}\begin{Bmatrix}T_{xz}\\ T_{yz}\end{Bmatrix}. \tag{B.19}$$

In the final phase of derivations the expression for the complementary transverse shear energy calculated from transverse shear stresses should be compared with the same energy but expressed by resultant shear forces:

$$\frac{1}{2}\int_{-\frac{h}{2}}^{\frac{h}{2}}\left(\left\{\boldsymbol{\sigma}_S\right\}^T\left[\mathbf{C}_S\right]^{-1}\left\{\boldsymbol{\sigma}_S\right\}\right)dz=\frac{1}{2}\begin{Bmatrix}T_{xz} & T_{yz}\end{Bmatrix}^T\begin{bmatrix}\tilde{a}_{55} & \tilde{a}_{45}\\ \tilde{a}_{45} & \tilde{a}_{44}\end{bmatrix}^{-1}\begin{Bmatrix}T_{xz}\\ T_{yz}\end{Bmatrix} \tag{B.20}$$

what finally, after using (B.19), brings the expression for the improved global transverse shear stiffness (which replaces the formula given (10)):

$$\begin{bmatrix}\tilde{a}_{55} & \tilde{a}_{45}\\ \tilde{a}_{45} & \tilde{a}_{44}\end{bmatrix}=\left[\int_{-\frac{h}{2}}^{\frac{h}{2}}\left(\begin{bmatrix}F_{11}(z) & F_{31}(z)\\ F_{32}(z) & F_{22}(z)\end{bmatrix}\left[\mathbf{C}_S\right]^{-1}\begin{bmatrix}F_{11}(z) & F_{32}(z)\\ F_{31}(z) & F_{22}(z)\end{bmatrix}\right)dz\right]^{-1}. \tag{B.21}$$